# 論文 / 著書情報
# Article / Book Information

| | |
|---|---|
| Title | Pairing strength in the relativistic mean-field theory determined from the fission barrier heights of actinide nuclei and verified by pairing rotation and binding energies |
| Authors | Taiki Kouno, Chikako Ishizuka, Tsunenori Inakura, Satoshi Chiba |
| Citation | Progress of Theoretical and Experimental Physics, Vol. 2022, Issue 2, |
| Pub. date | 2021, 12 |
| DOI | https://doi.org/10.1093/ptep/ptab167 |
| Creative Commons | Information is in the article. |

PTEP

Prog. Theor. Exp. Phys. **2022** 023D02(13 pages)
DOI: 10.1093/ptep/ptab167

# Pairing strength in the relativistic mean-field theory determined from the fission barrier heights of actinide nuclei and verified by pairing rotation and binding energies

Taiki Kouno, Chikako Ishizuka*, Tsunenori Inakura, and Satoshi Chiba

*Tokyo Institute of Technology, 2-12-1 Ookayama, Meguro, Tokyo 152-8550, Japan*
*E-mail: ishizuka.c.aa@m.titech.ac.jp

Received September 2, 2021; Revised November 30, 2021; Accepted December 17, 2021; Published December 21, 2021

We have studied the strength of the Bardeen–Cooper–Schrieffer (BCS) pairing force, used as a residual interaction to the relativistic mean-field approach, to reproduce the height of the inner fission barriers for actinide nuclei. It was found that increasing the pairing strength by about 13% makes the reproduction of the inner fission barriers better over a wide range of actinide nuclei. This result was verified by using the moment of inertia of the pairing rotational energy, which was introduced to avoid mean-field and odd-mass effects in the pairing interaction, to deduce purely the pairing strength. The pairing interaction thus determined could also improve the description of the binding energy of heavy nuclei. As a result, a consistent picture among inner fission barrier, binding energy, and pairing moment of inertia could be obtained in terms of the relativistic mean-field + BCS theory for a broad region of the actinide nuclei.

Subject Index D01, D06, D12, D26

## 1. Introduction

Nuclear fission is a process where a mono-nucleus turns into two smaller fragments, occasionally associated with the emission of a few neutrons or light charged particles. This phenomenon is important for applications in nuclear technologies due to the large Q-values and the possibility of sustaining chain reactions mediated by neutrons, and also for fundamental science such as r-process nucleosynthesis in the cosmos. However, it is still a mysterious physics phenomenon as a large-amplitude collective motion of finite nucleon systems [1]. The first theoretical analysis was carried out by Bohr and Wheeler, who introduced the important concept of fissility and predicted the existence of a fission barrier that corresponds to the activation energy of chemical reactions [2]. In their analysis they used the liquid-drop model of nuclei which predicts that there is only one barrier, or saddle point, in the complex potential-energy landscape in the multidimensional space of collective variables characterizing the nuclear shape during the fission process. In the contemporary understanding of nuclear fission for the actinide region, where experimental data are most abundant, it is known that nuclear fission occurs over the fission barrier, which typically has a two-humped structure, namely, over the inner and the outer barriers [3]. From an extensive amount of theoretical analysis, we now understand that the inner fission barrier is located in a space of deformation parameters where the mass asymmetry is

not important, but it is important for the outer barrier. Also, it is reported that the effect of triaxiality is present for the inner barrier, though its effect on the fission barrier heights is small (typically less than 1 MeV) in the macro–micro model [3,4] and some microscopic models [5–9]. However, in calculations using the relativistic mean-field (RMF) + point-coupling model of Refs. [10–13], the inner barrier is reduced by about 2 MeV by considering triaxiality, and therefore this effect is noticeable. In this manner, the effect of triaxiality on the inner fission barrier is highly model dependent and its quantitative value is uncertain. Furthermore, calculating the inner fission barrier without incorporating triaxiality not only saves computational time, but also makes sense since many computer programs used in applications assume axial symmetry (e.g. SkyAx [14] and the two-center shell model [15]). Therefore, we deal with the properties of the inner fission barrier ignoring triaxiality as the first step of this study. We understand that inclusion of triaxiality is definitely important for the quantitative calculation of fission barriers, but it will be left as a subject for future work.

The fission barrier has also been calculated in non-relativistic frameworks [16,17]. Besides the phenomenological ones whose parameters can be adjusted to observables, many non-relativistic microscopic approaches are based on Hartree–Fock theory with Skyrme [18] or Gogny forces [19] or density-functional theory. Those interactions (or functionals) are adjusted to reproduce the experimental data of ground-state properties, and have achieved great success in reproducing not only the properties of nuclear matter but also binding energies, nuclear radii, and neutron skin thickness over a wide range of nuclei systematically. The pairing interaction is included as a residual interaction in the Bardeen–Cooper–Schrieffer (BCS) or Bogoliubov form. In spite of the success in explaining ground-state properties, however, prediction of the fission barriers has remained quite poor. In many cases, the fission barriers for actinides are overestimated by 2 to 5 MeV [18,19], and it has been difficult to balance the reproduction of the fission barriers and the predictions for the ground-state properties.

The parameters describing the mean-field effects should be determined to reproduce the global properties of many nuclei, so must not be adjusted to local properties of nuclei. On the other hand, the parameters for the pairing interaction could be determined in a narrow region of nuclei, or ultimately nucleus by nucleus, since they describe the residual interaction. Moreover, the parameters for the pairing interaction have previously been determined from experimental data on the gap parameters and/or even–odd staggering of nuclear properties [5]. However, these methods are associated with ambiguities coming from the facts that (i) the gap parameter and the even–odd staggering are affected by the mean-field properties, and (ii) there is an ambiguity in the microscopic calculation of odd nuclei that breaks the time-reversal symmetry. A special treatment like the blocking method is also necessary in the calculation for odd nuclei, but it may introduce extra sources of uncertainty. A novel method, therefore, should be used to determine the parameters in the pairing interaction to avoid pollution by the mean-field effects and/or debatable methods of calculation for odd nuclei.

In this work, we propose a method to determine the BCS pairing interaction strengths [6] for actinide nuclei to reproduce the height of the inner fission barrier in the relativistic mean-field theory [20]. Our emphasis is to validate the pairing interaction thus determined by considering the "pairing moment of inertia" [21,22], which gives a property of the pairing interaction avoiding much of the mean-field effects and is determined using information only from a set of even–even nuclei. It has been pointed out that the pairing moment of inertia is an excellent experimental observable for maintaining time-reversal symmetry and measuring pair

correlation properly [21,22]. In addition, we verify that the pairing interaction determined here can provide a better prediction for the ground-state binding energies, pairing moment of inertia, and fission barrier heights simultaneously.

Our paper is organized as follows. In Sect. 2 we introduce the relativistic mean-field theory, pair correlation, and pairing rotation energy. In Sect. 3.1, we first look at the changes in the inner fission barrier when the pair correlation force is changed, taking $^{240}$Pu as an example, and evaluate the change in the pair rotation energy according to the change of the pair correlation force. In Sect. 3.2, the scope of investigation is expanded to a broader region of actinide nuclei, and the pair correlation force that reproduces the experimental inner fission barriers is obtained by referring to the Reference Input Parameter Library (RIPL-3) [23]. This is a highly important database for theoreticians involved in the development and use of nuclear reaction modeling (ALICE [24], EMPIRE [25], GNASH [26], UNF [27], TALYS [28], CCONE [29], and so on) for both theoretical research and nuclear data evaluations. In addition, RIPL-3 is often used to compare experimental and theoretical values of a wide variety of nuclear quantities. Furthermore, by using this pair correlation force, we verify that the binding energy and also the pair rotation are simultaneously described better than the original pairing interaction. In other words, we have shown that the pair rotation can be used to determine the pairing strength in a systematic manner.

## 2. Method

### 2.1 *Relativistic mean-field theory*

We start with the Lagrangian density considering relativistic invariance,

$$\begin{aligned}\mathcal{L}_{\rm RMF} &= \bar{\psi}(i\gamma_\mu\partial^\mu - M)\psi + \frac{1}{2}\partial^\mu\sigma\,\partial_\mu\sigma - U(\sigma) - g_\sigma\bar{\psi}\psi\sigma \\ &\quad - \frac{1}{4}\Omega^{\mu\nu}\Omega_{\mu\nu} + \frac{1}{2}m_\omega^2\omega^\mu\omega_\mu - g_\omega\bar{\psi}\gamma^\mu\psi\omega_\mu + U(\omega) \\ &\quad - \frac{1}{4}\boldsymbol{R}^{\mu\nu}\cdot\boldsymbol{R}_{\mu\nu} + \frac{1}{2}m_\rho^2\boldsymbol{\rho}^\mu\cdot\boldsymbol{\rho}_\mu - g_\rho\bar{\psi}\gamma^\mu\boldsymbol{\tau}\psi\boldsymbol{\rho}_\mu \\ &\quad - \frac{1}{4}F^{\mu\nu}F_{\mu\nu} - e\bar{\psi}\gamma^\mu\frac{(1-\tau_3)}{2}\psi A_\mu, \end{aligned} \tag{1}$$

$$\Omega^{\mu\nu} = \partial^\mu\omega^\nu - \partial^\nu\omega^\mu, \quad \boldsymbol{R}^{\mu\nu} = \partial^\mu\boldsymbol{\rho}^\nu - \partial^\nu\boldsymbol{\rho}^\mu, \quad F^{\mu\nu} = \partial^\mu A^\nu - \partial^\nu A^\mu, \tag{2}$$

including the non-linear terms

$$U(\sigma) = \frac{1}{2}m_\sigma^2\sigma^2 + \frac{1}{3}b_2\sigma^3 + \frac{1}{4}b_3\sigma^4, \tag{3}$$

$$U(\omega) = \frac{1}{4}c_3(\omega_\mu\omega^\mu)^2 \tag{4}$$

as self-interaction terms [30–32]. Here, $M$ is the nucleon mass, $m_\sigma$, $m_\omega$, and $m_\rho$ denote the meson masses, and $g_\sigma$, $g_\omega$, and $g_\rho$ represent the meson–nucleon coupling constants. Furthermore, $\sigma$, $\omega^\mu$, $\boldsymbol{\rho}^\mu$, and $A^\mu$ indicate the scalar-isoscalar field, vector-isoscalar field, vector-isovector field, and photon field, respectively. The symbol $\psi$ represents the nucleon Dirac field consisting of four components. In the relativistic mean-field approach, however, the fluctuation of the meson field is ignored, as are the negative energy components (the so-called no-sea approximation). Furthermore, besides the non-linear self-interaction term of the $\sigma$-meson which has been commonly used, the non-linear self-interaction term of the $\omega$-meson, whose importance has been

**Table 1.** Parameter values used in NLV-20.

| $M$ (MeV) | $m_\sigma$ (MeV) | $m_\omega$ (MeV) | $m_\rho$ (MeV) | $g_\sigma$ | $g_\omega$ | $g_\rho$ | $b_2$ ($\mathrm{fm}^{-1}$) | $b_3$ | $c_3$ |
|---|---|---|---|---|---|---|---|---|---|
| 938.9 | 489.049 | 780.0 | 763 | 10.0518 | 12.9354 | 4.90748 | −12.7384 | −34.0567 | 20.0 |

suggested by relativistic Brueckner–Hartree–Fock (RBHF) theory in recent years [31], is included. For this sake, we used the NLV-20 parameter set [32] primarily, although the conclusion obtained in this work does not depend on the particular choice of parameter set.

The parameters of NLV-20 are shown in Table 1, adjusted to reproduce the binding energies of $^{16}$O, $^{40,48}$Ca, $^{56,58}$Ni, $^{88}$Sr, $^{90}$Zr, $^{112,124,132}$Sn, $^{146}$Gd, and $^{208}$Pb, the diffraction radii of $^{16}$O, $^{40,48}$Ca, $^{56,58}$Ni, $^{88}$Sr, $^{90}$Zr, $^{112,124}$Sn, $^{146}$Gd, and $^{208}$Pb, and the surface thicknesses of $^{16}$O, $^{40,48}$Ca, $^{90}$Zr, $^{112,124}$Sn, and $^{208}$Pb. The saturation density obtained with this parameter set is 0.151 $\mathrm{fm}^{-3}$, the binding energy per nucleon is 16.24 MeV, the incompressibility is 190 MeV, and the symmetry energy per nucleon is 42.1 MeV for symmetric nuclear matter. Note that the parameters were determined by the properties of spherical nuclei alone, ranging from $^{16}$O to $^{208}$Pb.

We used the Nilsson oscillators in the basis expansion and cylindrical coordinates for the calculations with NLV-20, and deformed harmonic oscillators in the basis in the DD-ME2 and DD-PC1 cases. For the numerical details, refer to Refs. [32,33].

The total energy was calculated by volume-integrating the energy density obtained as the (00) component of the energy–momentum tensor [20]. Then, corrections were given for the center-of-mass energy $E_{\mathrm{cm}} = \langle \hat{P}^2_{\mathrm{cm}} \rangle / 2AM$, where $\hat{P}_{cm}$ is the center-of-mass momentum operator [32], and the pairing energy as explained in the next subsection. In calculating the total energy as a function of the deformation to cover the inner fission barrier, we imposed a constraint on the quadrupole moment calculated from the nucleon density $\rho(\boldsymbol{r})$:

$$Q_{20} = \frac{1}{2}\sqrt{\frac{5}{4\pi}} \int d^3\boldsymbol{r}\rho(\boldsymbol{r})(2z^2 - x^2 - y^2). \tag{5}$$

## 2.2 *Pairing interaction*

The effective pairing interaction is parametrized by using the following local pairing energy functional [34]:

$$\varepsilon_{\mathrm{pair}} = \frac{1}{4} \sum_{q\in\{p,n\}} \int d^3\boldsymbol{r}\chi^*_q(\boldsymbol{r})\chi_q(\boldsymbol{r})G_q(\boldsymbol{r}), \tag{6}$$

where $\chi_q(\mathbf{r})$ is the local part of the pair density matrix,

$$\chi_q(\boldsymbol{r}) = -2\sum_{k>0} f_k u_{k,q} v_{k,q} \left|\phi_{k,q}(\mathbf{r})\right|^2, \tag{7}$$

$$f_k = \frac{1}{1 + \exp[(\epsilon_k - \lambda_q - \Delta E_q)/\mu_q]}, \tag{8}$$

with $\phi_{k,q}$ the single-particle wave function for $q \in \{p, n\}$. The symbols $u_{k,q}$ and $v_{k,q}$ denote, respectively, the vacant and occupied amplitudes of a single orbit $k$ obtained by the BCS theory. Furthermore, $f_k$ are the energy-dependent cutoff weights, while $\Delta E_q$ and $\mu_q = \Delta E_q/10$ denote cutoff parameters [34]. In the present work we use a simple constant pairing strength, $G_q(\mathbf{r}) = G_q$, corresponding to the delta pairing interaction. The pairing strengths are taken from

Ref. [32]: $G_n = -348$ MeV fm$^3$ for neutrons and $G_p = -349$ MeV fm$^3$ for protons. These values are determined as follows. In Ref. [32], the pairing strengths were determined by reproducing the experimental pairing gaps of $^{44}$Ca, $^{106}$Sn–$^{128}$Sn, and $^{201}$Pb–$^{204}$Pb for neutrons, and $^{52}$Cr, $^{82}_{50}$Ge–$^{94}_{50}$Ru, $^{136}_{82}$Xe–$^{147}_{82}$Tb, and $^{212}_{126}$Rn–$^{215}_{126}$Ac for protons. Hereafter, a set of these numbers is denoted as $G = (-348, -349)$ [32].

### 2.3 *Pairing rotation*

In this work we adjust the strength of the pairing interaction to reproduce the height of the inner fission barriers of nuclei in the actinide region. Such a procedure can be justified only if the pairing strength thus determined is firmly consistent with the quantity related to the pairing correlation. Normally, the evaluation of the pair correlation is performed using the pairing gap and/or odd–even staggering of binding energy or neutron separation energy. But this method suffers from effects coming from the mean-field part, and also is difficult since it involves calculation for odd nuclei that break the time-reversal symmetry. Numerically, a special technique like the "blocking method" must be employed for calculating odd nuclei, which introduces extra ambiguity. Instead, we bring a concept called the moment of inertia of the "pairing rotation" [21,22]. This quantity can be evaluated using the binding energy of even–even nuclei alone, and hence is an excellent experimental observable for obtaining information on pair correlations that maintain time-reversal symmetry, while simultaneously reducing the mean-field effects.

The pairing rotation energy is defined by the following equation, derived by the pair correlation breaking the U(1) gauge symmetry [21,22]:

$$E(N, Z_0) = E(N_0, Z_0) + \lambda_n(N_0, Z_0)\Delta N + \frac{(\Delta N)^2}{2\mathcal{I}_{nn}(N_0, Z_0),} \tag{9}$$

where $E(N_0, Z_0)$ denotes the ground-state energy for a nucleus with neutron number $N_0$ and proton number $Z_0$, $\Delta N = N - N_0$, $\lambda(N_0) = dE/dN|_{N=N_0}$ is the chemical potential, and the second-order term is the pairing rotational energy with the pairing moment of inertia $\mathcal{I}_{nn}(N_0, Z_0)^{-1} = d^2E/dN^2|_{N=N_0}$. The pairing moment of inertia is given by the reciprocal of the second-order derivative of the energy around the $(N_0, Z_0)$ nucleus, which can be calculated by the following finite differentiation:

$$\mathcal{I}_{nn}^{-1}(N_0, Z_0) = \frac{E(N_0 + 2i, Z_0) + E(N_0 - 2i, Z_0) - 2E(N_0, Z_0)}{4i}, \tag{10}$$

where $i = 1$ is usually selected to calculate the second derivative of the pairing rotation energy by using nuclei with $N_0 - 2$, $N_0$, and $N_0 + 2$ neutrons, but for some cases $i = 2$ gives a better description of the second-order derivative, Eq. (9), or to discriminate different parametrizations. This quantity can be calculated by using the binding energy of even–even nuclei; the experimental values were taken from AME2016 [35].

## 3. Results and discussion

### 3.1 *Total energy*

In this paper we examine the influence of the pairing rotation for six actinides ($^{234}$U, $^{236}$U, $^{240}$Pu, $^{242}$Pu, $^{242}$Cm, and $^{244}$Cm) which are representative compound nuclei synthesized in neutron-induced reactions.

First, we show the dependence of the total energy of $^{240}$Pu on the quadrupole moment in three cases with pairing strengths $0.8G$, $G$, and $1.2G$. Here, $G$ is the original value

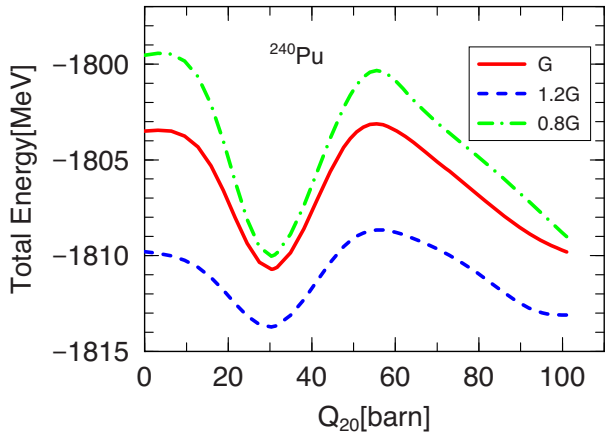


**Fig. 1.** The dependence of the total energy of $^{240}$Pu on the quadrupole moment for three values of the pairing strength parameters.

$G = (G_n, G_p) = (-348, -349)$ MeV fm$^3$. Since the original value $G$ was determined from even–odd mass staggering, which has an ambiguity in connection with the pairing strength, we adjusted the pairing strength to reproduce the heights of the inner fission barrier, and validated the results by other quantities, namely the moment of inertia of the pairing rotation and the binding energies. Furthermore, there is the possibility of adjusting $G_n$ and $G_p$ independently. However, we did not do this since we tried to minimize the extra freedom we introduced in this work.

Figure 1 shows how the total energy of $^{240}$Pu depends on $Q_{20}$ for three sets of pairing strengths. It can be seen that the position of the ground state stays at $Q_{20} \simeq 30$ barn, while the top of the inner barrier, namely, the saddle point, stays at $Q_{20} \simeq 60$ barn regardless of the strength of the pairing interaction. The height of the inner fission barrier was obtained as the difference between the energies of the saddle point and the ground state. The experimental value of the height of the inner fission barrier, taken from RIPL-3 [23], is 6.05 MeV, while the three values of the pairing strength yield the following three results:

$$G \to 7.54\,\text{MeV}, \qquad 1.2G \to 5.08\,\text{MeV}, \qquad 0.8G \to 9.71\,\text{MeV}. \tag{11}$$

Hereafter, we adjust the pairing strengths of both neutrons and protons by a single multiplier parameter $\alpha$ as $G \to \alpha G$. One of the reasons why the height of the inner fission barrier changes depending on the strength of the pairing force is due to the fact that the single-particle level densities around the Fermi surface are different at the ground state and the saddle point. This physical picture can be understood from Fig. 2, which depicts the neutron single-particle energies of $^{240}$Pu at the ground state and saddle point. Furthermore, from Fig. 3, which shows the deformation dependence of the pairing energy at each pairing strength, it is possible to know how the pairing energy works at each degree of deformation. In particular, these values are maximal at the GS (ground state), while they take minimal values at the saddle point. Such a physical picture can be understood intuitively by the following equation proposed in Ref. [36], which defines the difference between the energies of the correlated state $E(\Delta \neq 0)$ and the unpaired state $E(\Delta = 0)$:

$$E(\Delta) - E(0) \simeq -\frac{1}{2}\rho\Delta^2, \tag{12}$$

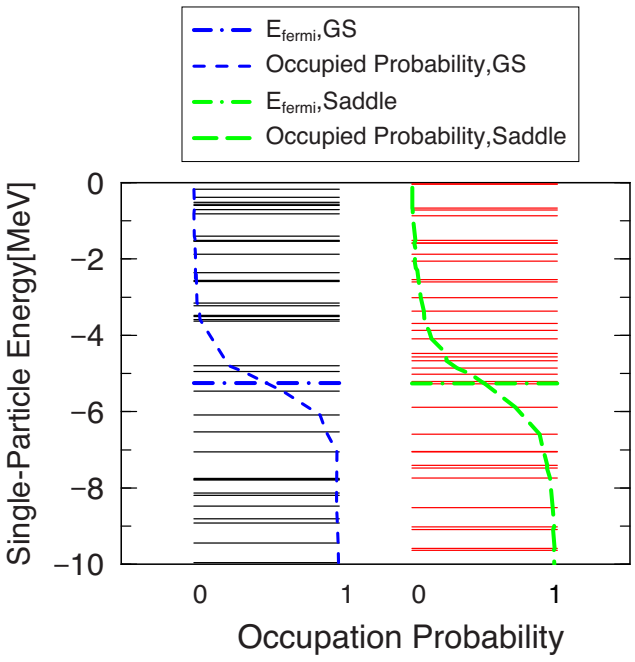


**Fig. 2.** The neutron single-particle energies of $^{240}$Pu at the ground state (left) and saddle point (right). In addition, the broken lines represent occupied probabilities at both points. The horizontal dot-dashed lines denote the Fermi energy (or chemical potential in BCS theory). Here, "GS" represents the ground states.

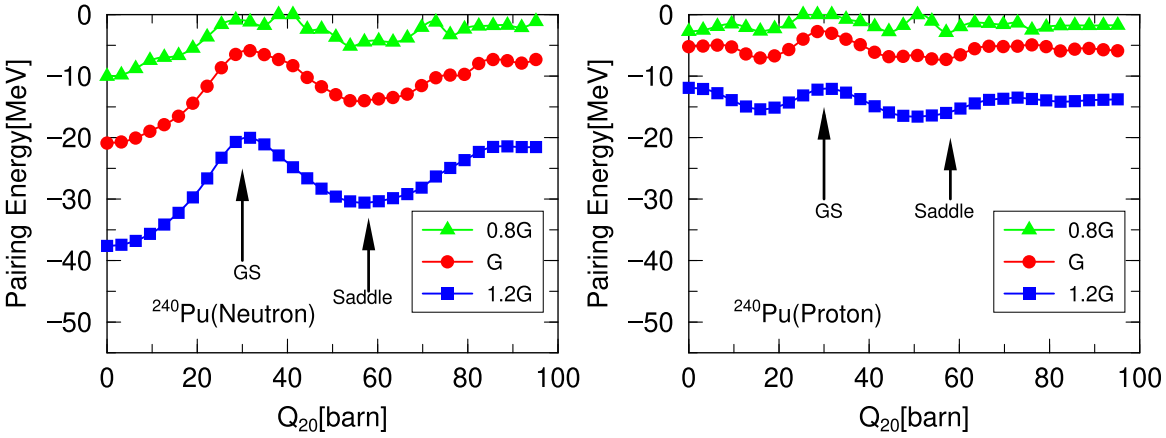


**Fig. 3.** The pairing energy of a neutron (left) and proton (right) of $^{240}$Pu as a function of the deformation by each pairing strength.

where $\Delta$ is the BCS gap parameter and $\rho$ is the level density. The gap $\Delta$ is also given approximately as

$$\Delta \sim 2S \exp\left(-\frac{1}{G_0\rho}\right), \tag{13}$$

which indicates that it increases as $\rho$ increases. Here, $S$ denotes an energy range where the $u$ and $v$ factors deviate noticeably from 0 and 1, respectively, and $G_0$ denotes the pairing strength in MeV when the pairing interaction is written in the form $H_{\rm pair} = G_0 \sum_\mu \sum_\nu a^\dagger_\mu a^\dagger_{\bar{\mu}} a_{\bar{\nu}} a_\nu$ [36]. From Eqs. (12) and (13) and Figs. 2 and Fig. 3, it can be seen that the pairing effect is stronger as a negative value at the saddle point than in the ground state since the level density is higher in the

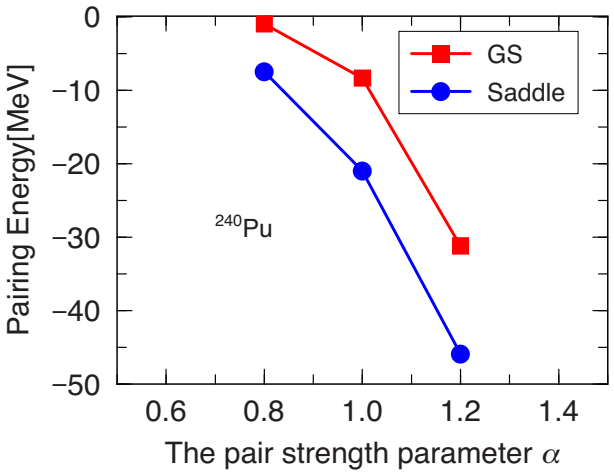


**Fig. 4.** The changes of pairing energy for each pair strength on the ground states and saddle point.

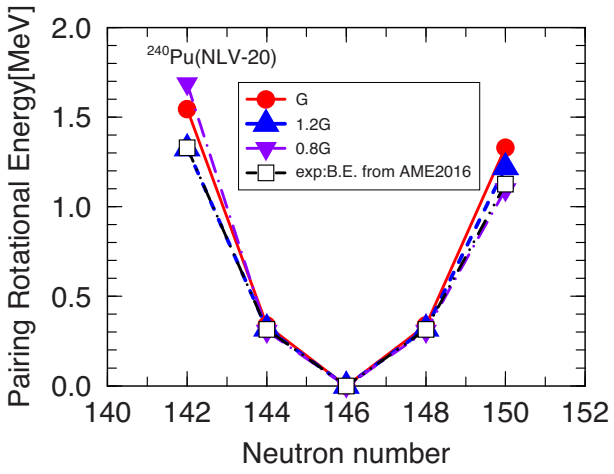


**Fig. 5.** The pairing rotation energy by changing the pairing strength in $^{240}$Pu with NLV-20.

former. We also notice that the change of the pairing energy is stronger for neutrons than for protons. Furthermore, as shown in Fig. 4, which depicts the changes of pairing energy for each pairing strength on ground states and saddle point, the slope of the pairing energy dependent on the pairing strength parameter $\alpha$ is steeper at the saddle point where the level density is higher. It is concluded that one of the reasons for the fission barrier changes is the effects of the pairing correlation. The above discussion was conducted with reference to Ref. [6], which also contains a more detailed analysis and discussion.

In this example, increasing the value of the pairing strength decreases the overall energy of the system, while the change is smaller at the ground state than at the saddle point. Accordingly, it changes the height of the inner fission barrier, and the agreement with the experimental value becomes better. The crucial point here, however, is whether or not the increase of the pairing strength gives a consistent picture, or better reproduction, for the pairing rotation. To see this, we plot the pairing rotation energy in Fig. 5. It can be seen that the experimental value of the pairing rotational energy around $^{240}$Pu is reproduced almost equivalently when the pairing strength is increased with the original pairing strength for $i = 1$ (see Eq. (10)), or better for the $i = 2$ case. In particular, it can be seen that the results for $0.8G$ and $G$ at $N = 142$ are

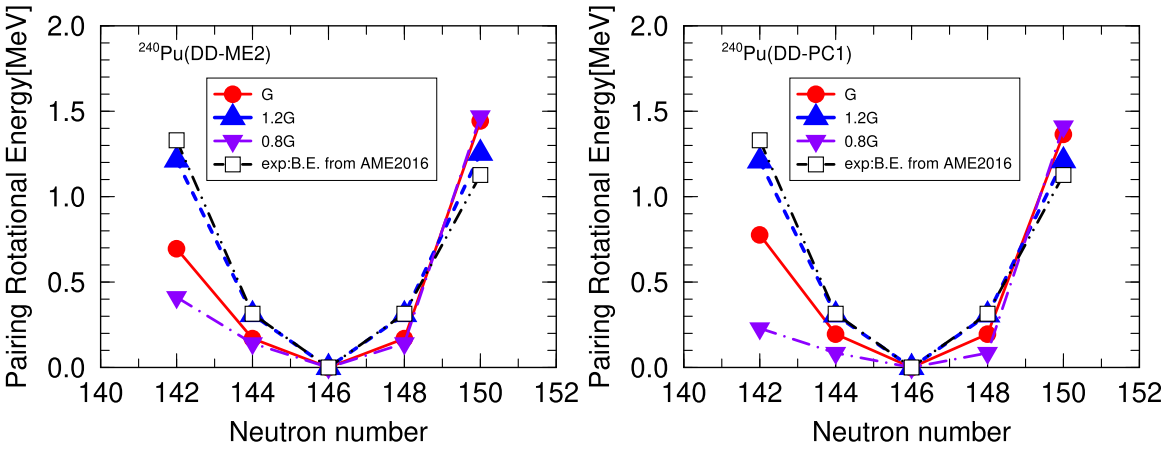


**Fig. 6.** The pairing rotation energy by changing the pairing strength in $^{240}$Pu with DD-ME2 [33,37] (left) and DD-PC1 [33,38] (right). Lines are drawn only as eye-guides, and only the values at even integer values of the neutron number have meaning.

significantly worse than $1.2G$. The deviation between the calculated pairing rotational energy at $N = 150$ seems to be smallest with $0.8G$. However, the total deviation in $N = 142$–$150$ becomes smallest with $1.2G$. Similar plots were made for different interactions, DD-ME2 [37] and DD-PC1 [38], in Fig. 6. In the latter two interactions, agreement with the measured pairing rotational energy is drastically improved when the pairing strength is increased by 20% compared with the original strength and the case where the pairing strength is reduced by 20%. The values of the fission barriers for the two latter, density-dependent, interactions with triaxiality taken into account are 7.50 and 6.53 MeV, respectively, which are still 1– 2 MeV too large compared to the measured value. This is the same situation as calculation with the NLV-20 interaction, without triaxiality. This result indicates a procedure to increase the pairing strength in the actinide region to better reproduce the values of the inner fission barrier. Therefore, we will proceed to perform a systematic analysis in this direction by adopting the NLV-20 interaction in the following.

### 3.2 *Pairing strength*

From the preceeding analysis, we found that the fission barrier can be adjusted by changing the pairing strength, while making agreement with the pairing rotational energy much better than using the original pairing strength, as shown in Figs. 5 and 6. Therefore, we selected six nuclei ($^{234}$U, $^{236}$U, $^{240}$Pu, $^{242}$Pu, $^{242}$Cm, and $^{244}$Cm) from the actinide region for which the moment of inertia of the pairing rotation can be defined well, and determined the pair correlation force that reproduces the experimental values of the inner fission barriers taken from RIPL-3 [23]. Such pairing strengths adjusted to reproduce the inner fission barrier are denoted as $G_{\rm best} \equiv \alpha \cdot G$ and the pair strength parameter values $\alpha$ are shown in Fig. 7 as a function of $Z^2/A^{1/3}$ for the fissioning nuclei. A straight line assuming a weak dependence on $Z^2/A^{1/3}$ is drawn, but it is almost equivalent with the average $\alpha$ value of 1.127.

We calculated the root-mean square (RMS) error by

$$RMS = \sqrt{\sum_{i=1}^{6} \frac{\left(x_i^{\rm th} - x_i^{\rm exp}\right)^2}{6}}, \quad \{x_i \equiv B_f,\ \text{binding energy},\ \mathcal{I}_{nn} \text{ for the } i\text{th nucleus}\}, \quad (14)$$

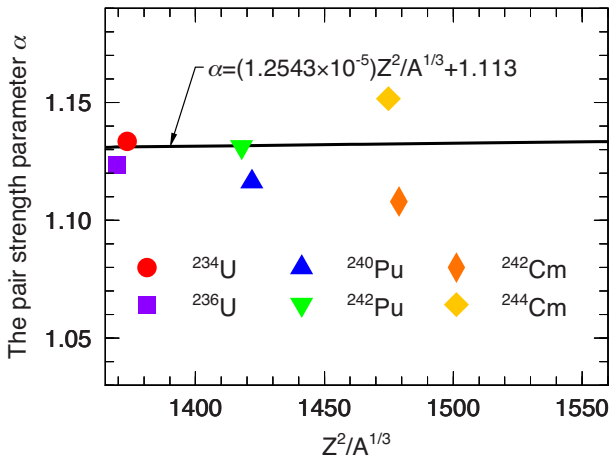


**Fig. 7.** The pair strength parameter $\alpha$ with $Z^2/A^{1/3}$. The solid line is a linear fit to $\alpha$, and $G_{\rm best} = \alpha$(for each nucleus) $\cdot\, G$.

**Table 2.** RMS error by $G$ and $G_{\rm best}$.

| | $G$ | $G_{\rm best}$ |
|---|---|---|
| $B_f$ MeV | 1.39 | — |
| Binding energy (MeV) | 2.84 | 1.43 |
| $\mathcal{I}_{nn}$ (MeV$^{-1}$) | 1.43 | 1.20 |

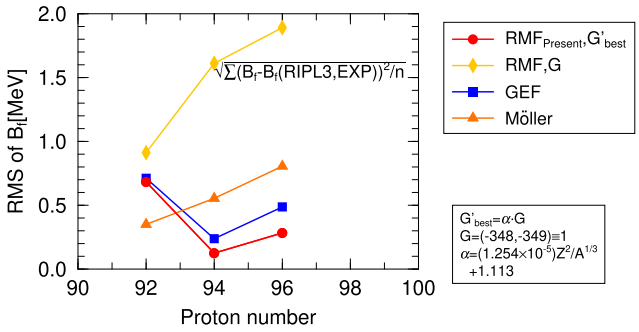


**Fig. 8.** RMS for the fission barrier, with RIPL-3 taken as the standard.

where $x_i^{\rm th}$ and $x_i^{\rm exp}$ denote the theoretical and experimental values, respectively. Table 2 summarizes the RMS errors of the three quantities depending on the pairing force strength. It should be noted that the binding energy calculated with $G_{\rm best}$ becomes better for all the nuclides considered: the RMS error is improved by about 50%. Similarly, it can be seen that the pairing moment of inertia is also improved by calculation with $G_{\rm best}$, resulting in the RMS error being reduced by more than 16%.

In the following, we use the linear fit of the $\alpha$ value as shown in Fig. 7 to calculate the systematic properties in the actinide region.

First, we compare the RMS values of the inner fission barrier height from two sources (GEF [39] and Möller [40]) and present the RMF (original $G$ and $G'_{\rm best} = \alpha \cdot G$ with $\alpha$ given as a linear fit) against the experimental data given in RIPL-3 [23] for $Z = 90$, 92, and 94 elements in Fig. 8. What is clear is that Möller's RMS of the barrier calculated by the macroscopic–microscopic

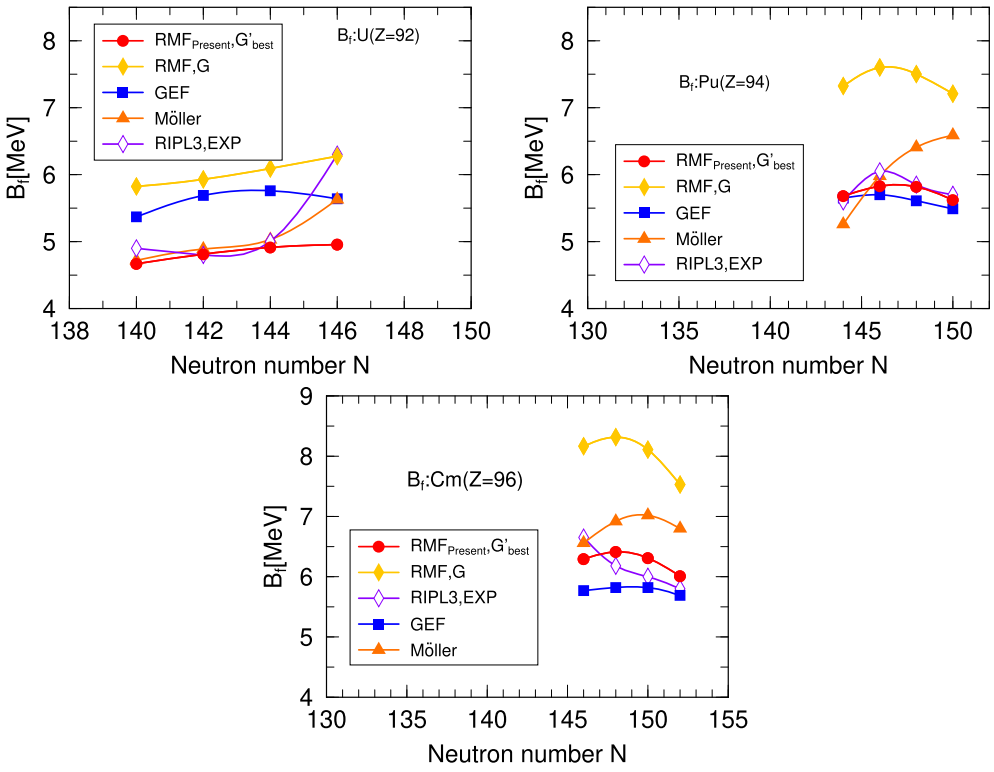


**Fig. 9.** Comparison of the calculation results for inner fission barrier by RMF (linear fit to $G'_{\rm best}$ with RMF ($G$), GEF, Möller, and RIPL-3.

model and RMF ($G$) behaves differently from GEF and RMF ($G'_{\rm best}$). The RMF ($G'_{\rm best}$) result for uranium ($Z = 92$) has a large RMS due to the inability to reproduce the bouncing behavior of $^{238}$U (see Fig. 9). It was found that $G'_{\rm best}$ calculated here gives a small RMS overall, especially for Pu and Cm isotopes.

Next, the calculated inner fission barrier heights by RMF ($G'_{\rm best} = \alpha \cdot G$, where $\alpha$ is given by a linear fit) and RMF ($G$) are compared for each element in Fig. 9. It can be seen that for nuclides other than $^{238}$U, the agreement with the data (open purple diamonds) is improved by about 2 MeV by calculations with $G'_{\rm best}$ (red filled circles) than those with $G$ (filled yellow diamonds). A comparison of the inner fission barrier obtained by using $G'_{\rm best}$ with other literature values (GEF [39] (blue filled squares) and Möller [40] (orange filled triangles)) is also shown in this figure. We recognize that the present RMF calculation with $G'_{\rm best}$ reproduces the fission barrier height quite well compared to other calculations. The $B_f$ of $^{238}$U shows a sudden jump from that of $^{236}$U, but this behavior could not be reproduced by the present parametrization given by a linear function of $Z^2/A^{1/3}$. Otherwise, the present parametrization shows an overall agreement with experimental data for other isotopes of U and all the Pu and Cm isotopes.

The changes in the description of the binding energies and moment of inertia of pairing rotation $\mathcal{I}_{nn}$ calculated with $G$ and $\alpha \cdot G$ where $\alpha$ is given by the linear fit in Fig. 7 are indicated in Table 3. As we can see, the RMS errors for both quantities were reduced noticeably. It is especially interesting that the improvements in the binding energies are significant, since the RMF parameters were originally determined to reproduce the binding energies of lighter nuclei, so we may expect that there is a little room to improve the description of the binding energies.

**Table 3.** Binding energy and moment of inertia of pairing rotation for $G$ and $G'_{\rm best}$.

| | RMS(B.E.) (MeV) | | RMS($\mathcal{I}_{nn}$) (MeV$^{-1}$) | |
|---|---|---|---|---|
| Element | $G$ | $G'_{\rm best}$ | $G$ | $G'_{\rm best}$ |
| Uranium | 3.450 | 1.934 | 1.022 | 0.840 |
| Plutonium | 3.757 | 2.226 | 1.182 | 0.756 |
| Curium | 3.377 | 1.905 | 2.471 | 1.788 |

## 4. Summary

We systematically investigated the height of the inner fission barrier of actinide nuclei using BCS pair correlation as a residual interaction in relativistic mean-field theory. In all of the NLV-20, DD-ME2, and DD-PC1 parametrizations, the inner fission barrier was overestimated by 1–2 MeV for $^{240}$Pu. On this basis, the experimental values of the inner fission barrier could be reproduced better by appropriately enhancing the pair correlation force by about 13%, and new systematics of the pairing strength was constructed for NLV-20 as a linear fit that can be applicable to nuclei in the actinide region. In addition, we introduced the concept of pair rotation, which has been pointed out recently as a method for purely evaluating the pair correlation effects compared to the conventional method, and validated the pairing strength adjusted to reproduce the inner fission barrier. As a result, consistent results were obtained in which not only the inner fission barrier heights but also the accuracy of the binding energy and the pair rotation moment of inertia were improved simultaneously, and this new systematics can be used for predictions of various quantities in the actinide region. Although our results were obtained in terms of the constant pairing strength in the relativistic mean-field theory, the same trend can be concluded for a density-dependent pairing interaction, or even for non-relativistic approaches such as the Skyrme–Hartree–Fock method. It must also be pointed out that the inclusion of triaxiality will change the value of the $\alpha$ parameter given as a linear fit, but the essential conclusions should remain unchanged.

**Acknowledgments**

The authors are grateful to Prof. J. Maruhn (Goethe University Frankfurt) for essential support in carrying out this study.

## References

[1] M. Bender et al., J. Phys. G: Nucl. Part. Phys. **47**, 113002 (2020).
[2] N. Bohr and J. A. Wheeler, Phys. Rev. **56**, 426 (1939).
[3] S. Bjørnholm and J. E. Lynn, Rev. Mod. Phys. **52**, 725 (1980).
[4] A. Baran and K. Pomorski, Nucl. Phys. A **361**, 83 (1981).
[5] K. Rutz, J. A. Maruhn, P. G. Reinhard, and W. Greiner, Nucl. Phys. A **590**, 680 (1995).
[6] S. Karatzikos, A. V. Afanasjev, G. A. Lalazissis, and P. Ring, Phys. Lett. B **689**, 72 (2010).
[7] H. Abusara, A. V. Afansjev, and P. Ring, Phys. Rev. C **82**, 044303 (2010).
[8] S. E. Agbemava, A. V. Afanasjev, D. Ray, and P. Ring, Phys. Rev. C **95**, 054324 (2017).
[9] Z. Shi, A. V. Afanasjev, Z. P. Li, and J. Meng, Phys. Rev. C **99**, 064316 (2019).
[10] B. N. Lu, E. G. Zhao, and S. G. Zhou Phys. Rev. C **85**, 011301(R) (2012).
[11] B. N. Lu, J. Zhao, E. G. Zhao, and S. G. Zhou, Phys. Rev. C **89**, 014323 (2014).
[12] J. Chao, B. N. Lu, T. Niksic, D. Vretenar, and S. G. Zhou, Phys. Rev. C **93**, 044315 (2016).
[13] V. Prassa, T. Niksic, G. A. Lalazissis, and D. Vretenar, Phys. Rev. C **86**, 024317 (2012).
[14] P.-G. Reinhard, B. Schuetrumpf, and J. A. Maruhn, Comput. Phys. Commun. **258**, 107603 (2021).

[15] J. A. Maruhn and W. Greiner, Z. Phys. **251**, 431 (1972).
[16] A. Baran, M. Kowal, P.-G. Reinhard, L. M. Robledo, A. Staszczak, and M. Warda, Nucl. Phys. A **994**, 442 (2015).
[17] J. Sadhukham, J. Dobaczewski, W. Nazarewicz, J. A. Sheikh, and A. Baran, Phys. Rev. C **90**, 061304 (2014).
[18] K. Kean, T. Nishikawa, and Y. Iwata, JPS Conf. Proc. **32**, 010018 (2020).
[19] R. Rodriguez-Guzman, Y. M. Humadi, and L. M. Robledo, Eur. Phys. J. A **56**, 43 (2020).
[20] B. D. Serot and J. D. Walecka, Adv. Nucl. Phys. **16**, 1 (1986).
[21] N. Hinohara and W. Nazarewicz, Phys. Rev. Lett. **116**, 152502 (2016).
[22] D. M. Brink and R. A. Broglia, Nuclear Superfluidity, Pairing in Finite Systems (Cambridge University Press, Cambridge, 2005).
[23] R. Capote et al., Nucl. Data Sheets **110**, 3107 (2009).
[24] M. Blann, ALICE-91, Statistical Model Code System with Fission Competition, RSIC Code Package PSR-146 (1991).
[25] M. Herman, R. Capote, B. V. Carlson, P. Oblozinsky, M. Sin, A. Trkov, H. Wienke, and V. Zerkin, Nucl. Data Sheets **108**, 2655 (2007).
[26] P. G. Young and E. D. Arthur, GNASH: A preequilibrium, statistical nuclear model code for calculation of cross sections and emission spectra, [In FORTRAN for CDC 7600], LA-6947 (1977). https://doi.org/10.2172/5224192.
[27] J. Zhang, Nucl. Sci. Eng. **142**, 207 (2002).
[28] A. J. Koning and D. Rochman, Nucl. Data Sheets **113**, 2841 (2012).
[29] O. Iwamoto, N. Iwamoto, S. Kunieda, F. Minato, and K. Shibata, Nucl. Data Sheets **131**, 259 (2016).
[30] S. Gmuca, Nucl. Phys. A **547**, 447 (1992).
[31] Y. Sugahara and H. Toki, Nucl. Phys. A **579**, 557 (1994).
[32] K. Rutz, PhD dissertation, Johann Wolfgang Goethe-Universität, Frankfurt am Main (1999).
[33] T. Niksic, D. Vretenar, N. Paar, and P. Ring, Comput. Phys. Commun. **185**, 1808 (2014).
[34] M. Bender, K. Rutz, P.-G. Reinhard, and J. A. Maruhn, Eur. Phys. J. A **8**, 59 (2000).
[35] W. J. Huang, G. Audi, Meng Wang, F. G. Kondev, S. Naimi, and X. Xu, Chin. Phys. C **41**, 030002 (2017).
[36] S. G. Nilsson and I. Ragnarsson, Shapes and Shells in Nuclear Structure (Cambridge University Press, Cambridge, 1995).
[37] G. A. Lalazissis, T. Niksic, D. Vretenar, and P. Ring, Phys. Rev. C **71**, 024312 (2005).
[38] T. Niksic, D. Vretenar, and P. Ring, Phys. Rev. C **78**, 034318 (2008).
[39] K.-H. Schmit, B. Jurado, C. Amouroux, and C. Schmitt, Nucl. Data Sheets **131**, 107 (2016).
[40] P. Moller, A. J. Sierk, T. Ichikawa, A. Iwamoto, R. Bengtsson, H. Uhrenholt, and S. Aberg, Phys. Rev. C **79**, 064304 (2009).